Available online at www.sciencedirect.com
ScienceDirect
Materials Letters 62 (2008) 1458–1461
materials letters
www.elsevier.com/locate/matlet

Reaction-crystallization growth and electrical property of ammonium decavanadate nanorods

Liqiang Mai, Chunhua Han *

School of Materials Science and Engineering, Wuhan University of Technology, Wuhan 430070, China

Received 31 May 2007; accepted 28 August 2007
Available online 11 September 2007

Abstract

Ammonium decavanadate single crystalline nanorods with an average diameter of 100 nm, length up to 5 μm, was synthesized at a large scale in an ammonium metavanadate solution by a direct reaction-crystallization growth route. Investigations were conducted by XRD, DSC/TG, Raman, SEM, EDS, TEM, SAED and electrical transport along single nanorod. The results show that ammonium decavanadate nanorods grow along the direction of [1–21]. The individual nanorod exhibits nonlinear current/voltage (*I*/*V*) characteristics, with a conductivity of 0.15 S/cm at room temperature. The dominant conduction mechanism is based on small polaron hopping between V^{5+} and V^{4+} impurity centers and the *I*–*V* curve consists of a linear, Ohmic regime at lower electrical field and a nonlinear one at higher electrical field.

Keywords: Ammonium decavanadate; Nanorods; Electrical property

1. Introduction

In recent years, it is more and more attractive for many researchers to explore the design of a great variety of interesting materials with tailored morphologies owing to the prospect of using nanostructured objects as components in nanotechnology [1–3]. Among them, nanorods are of considerable interest as functional units for mediating the transport of electrons or optical excitations [4]. Vanadium oxide and their derivated compounds have attracted much attention due to their outstanding structural flexibility combined with chemical and physical properties, and also because of potential applications in areas such as catalysts, high-energy lithium batteries, chemical sensors, electrical and optical devices [5–7]. Recently, various methods have been developed to synthesize the nanorod materials of vanadium oxide and their derivated compounds. However, only limited kinds of single-crystal vanadates with 1-D nanostructures are obtained until now, and the synthesis of new-type nanorods remains challenging [8]. Herein, we report the reaction-crystallization synthesis and electrical property of ammonium decavanadate single crystalline nanorods.

2. Experimental

A light yellow clear solution was attained by dissolving ammonium metavanadate in deionized water. HCl acid was added dropwise to the above solution (0.14 mol/L) until the final pH was 1–2 under stirring. After ultrasonic treatment for 5 min, an orange solution was attained and then transferred into a 100-mL Teflon-lined autoclave with a stainless-steel shell, which was maintained at 180 °C for four days and then cooled at room temperature. The final precipitate was collected and washed with deionized water to remove any other residues and then dried in air at 80 °C for 6–8 h. The products were characterized on a Shimadzu XD-3A X-ray diffraction (XRD) with graphite monochromatized Cu Karadiation ($\lambda = 0.15148$ nm) and nickel filter. The Raman spectra were taken on a Renishaw RM-3000 laser Raman microscope system. Scanning electron micrograph (SEM) images of the samples were obtained in a JEOL JSM-5610LVS scanning electron microscope. Transmission electron microscope (TEM) images and selected area diffraction (SAED) pictures were recorded on a JEOL-JEM 200CX transmission electron microscope (200 KV). Differential scanning calorimetric analysis (DSC) and thermogravimetric analysis (TGA) were carried out with Labsys™ TG-DTA/DSC apparatus (SETARAM) with a heating rate of 10 °C/min in flowing air. The fabrication of a single ammonium decavanadate

* Corresponding author.
E-mail address: hch5927@whut.edu.cn (C. Han).

0167-577X/$ - see front matter © 2007 Elsevier B.V. All rights reserved.
doi:10.1016/j.matlet.2007.08.088

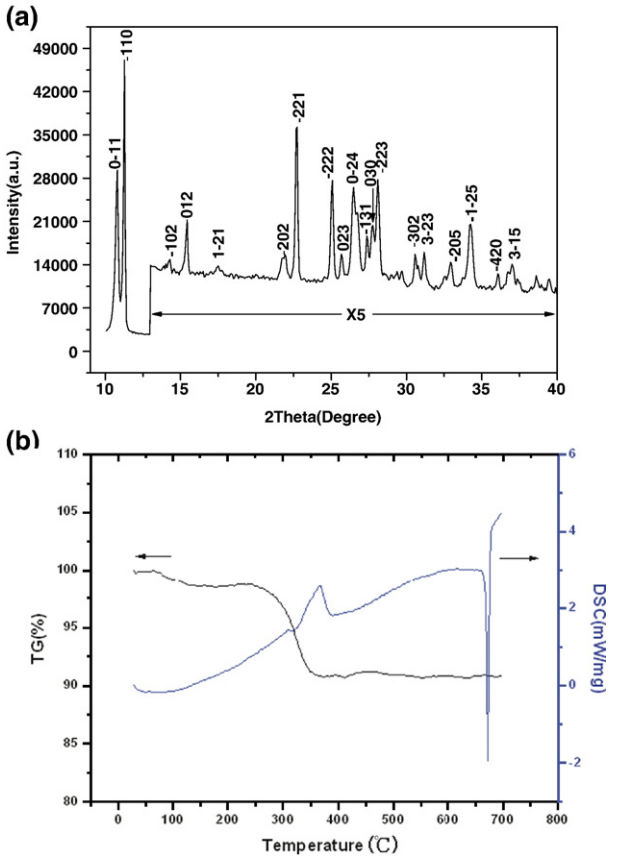

Fig. 1. (a) XRD pattern of the products. The intensity from 13 to 40° for 2θ angle is magnified by 5 times for clarity purpose. (b) TG and DSC curves of the $(NH_4)_6V_{10}O_{28}{\cdot}6H_2O$ nanorods in air.

nanorod based device was carried out by ac electrophoresis and focused ion beam (FIB) techniques [9]. DS345 Function Generator by Stanford Research System was used to test the electrical properties.

3. Results and discussion

The XRD pattern of the as-synthesized products is shown in Fig. 1a. All diffraction peaks can be readily indexed to the anorthic system with the lattice constants $a=10.15$ Å, $b=10.28$ Å, $c=16.73$ Å, ∝a" was changed to "α". Please check if appropriate.–>=96.5°, $\beta=87.18°$, $\gamma=8.99°$ (JCPDS No. 79-1789). No peaks of any other phases are detected, indicating the high purity of the $(NH_4)_6V_{10}O_{28}{\cdot}6H_2O$ products.

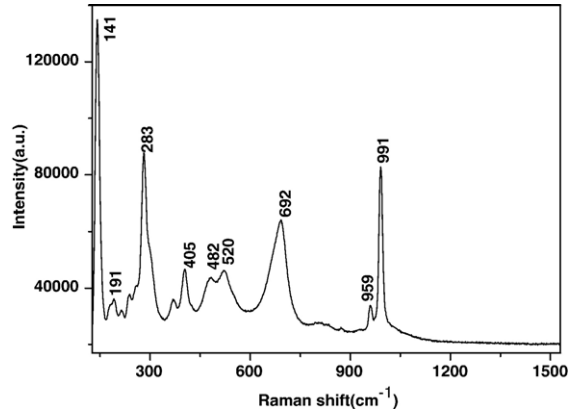

Fig. 2. Raman spectrum of the $(NH_4)_6V_{10}O_{28}{\cdot}6H_2O$ nanorods in room temperature.

Table 1
Raman peak frequencies and attributions of phonons in $(NH_4)_6V_{10}O_{28}{\cdot}6H_2O$ nanorods and bulk V_2O_5

$(NH_4)_6V_{10}O_{28}{\cdot}6H_2O$ nanorods/cm^{-1}	V_2O_5/cm^{-1}	Attribution[a]
141	146	$\delta(O_2V_2)n$
191	198	$\delta(O_2V_2)n$
283	258	δ(O–V)
303	305	δ(O–V_3)
405	406	δ(O–V)
482	483	δ(O–V_2)
520	528	ν(O–V_3)
692	702	ν(O–V_2)
959	913	ν(O–V)
991	996	ν(O–V)

[a] ν: stretching mode; δ: bending mode; $(O_2V_2)n$: VO_x layered structure; (O–V): terminal oxygen (V–O) structure; (O–V_2): doubly coordinated oxygen structure; (O–V_3): triply coordinated oxygen structure.

TG measurement (Fig. 1b) reveals a 9.1% weight loss from 65 to 380 °C, which originates from the decomposition of $(NH_4)_6V_{10}O_{28}{\cdot}6H_2O$ to V_2O_5 confirmed by XRD investigation (not shown here), corresponding to the following reaction

$$(NH_4)_6V_{10}O_{28}\cdot 6H_2O \rightarrow 5V_2O_5 + 6NH_3(g) + 9H_2O(g). \quad (1)$$

This weight loss matches very well the water and ammonium content of $(NH_4)_6V_{10}O_{28}{\cdot}6H_2O$ (9.2%). In addition, as shown in the DSC curve, the endothermic peak at 316 °C and the exothermic peak at 366 °C correspond to the dehydration and the decomposition of ammonium, respectively. And the endothermic peak at 673 °C shows melts-point of the V_2O_5 from the decomposition of $(NH_4)_6V_{10}O_{28}{\cdot}6H_2O$. When temperature is more than 673 °C, tiny weight loss of the samples can be attributed to vaporization of V_2O_5. The TGA/DSC results further confirm that the product is $(NH_4)_6V_{10}O_{28}{\cdot}6H_2O$.

From Fig. 2 and Table 1, it is shown that the Raman peaks at 285, 305, 406, 483, 528, 702, 996 cm^{-1} have a red shift of less than 10 cm^{-1}, which should be attributed to both the quantum confinement effect (QCE) [10]. The frequency shift of vanadyl mode is also ascribed to the presence of ammonium cations in the vicinity of oxygen and to the distortion of the V═O bonds [11]. Notably, the terminal oxygen symmetric stretching mode of V═O at 913 cm^{-1} shifts to higher wavenumber of 959 cm^{-1}. This chemical shift could be related to the reduction of oxidation state of vanadium from V^{5+} to V^{4+} and the increase of electronic conductivity [11]. Although the presence of V^{4+} needs to be confirmed by electron paramagnetic resonance (EPR) technique, the increase of electronic conductivity has been supported by the electrical test results below.

SEM investigation shown in Fig. 3a–b indicates that the resulting products is composed mainly of rod-like nanostructures with well-defined facets and the texture-like structure of the nanorods can be seen clearly. The average diameter of the nanorods is 100 nm, with lengths of 1–5 μm. Energy dispersive X-ray spectroscopy (EDS) further confirms the presence of N, V and O (H cannot be detected by EDS). The yield of the nanorods is estimated to be higher than 90% based on the SEM result.

TEM result (Fig. 3d) further reveals that the smaller rods with diameters ranging from 40 to 80 nm are agglomerated to form the typical bundle structures which corresponds to the texture-like morphology as seen by SEM. The SAED pattern taken from a single nanorod (Fig. 3e) is indexed to anorthic $(NH_4)_6V_{10}O_{28}{\cdot}6H_2O$. Significantly, the diffraction

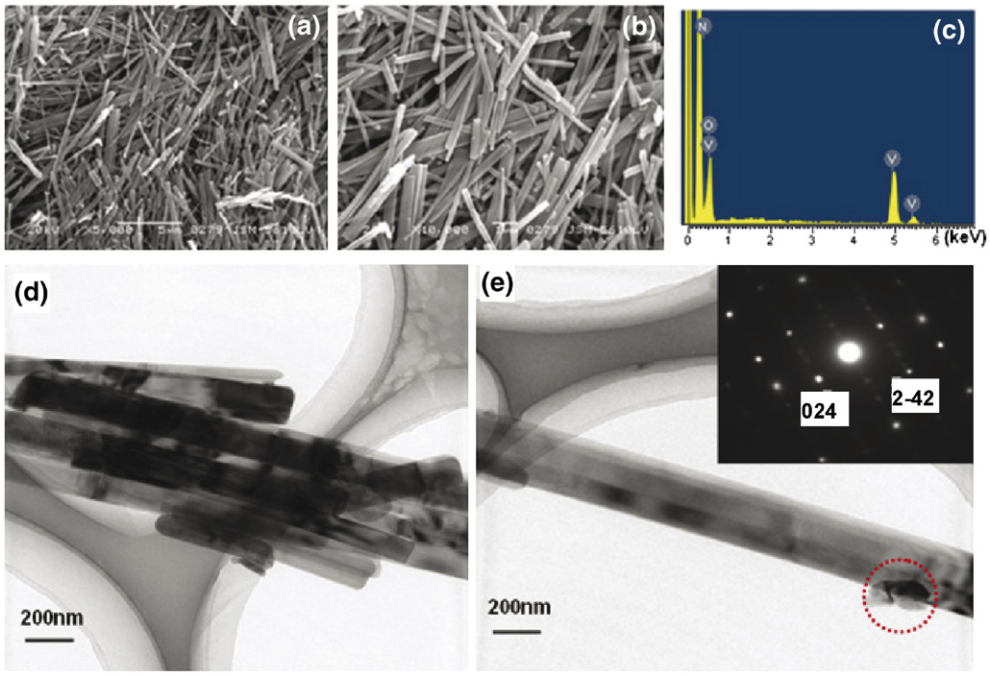

Fig. 3. Low (a) and high magnification (b) SEM images, EDS spectrum (c) of $(NH_4)_6V_{10}O_{28}\cdot 6H_2O$ nanorods; TEM images of the $(NH_4)_6V_{10}O_{28}\cdot 6H_2O$ nanorods bundle (d) and a single nanorod (the inset shows the corresponding SAED pattern) (e).

pattern did not change as the electron beam was moved along the nanorod, indicating that the whole nanorod is a single crystal, with a preferential growth direction along the [1–21] direction.

The *I–V* curve of the individual $(NH_4)_6V_{10}O_{28}\cdot 6H_2O$ nanorods at room temperature is shown in Fig. 4a. A contact resistance is about 80 MΩ, the effective length and cross-section of the sample is known only at approximately 4.7×10^{-4} cm and 4×10^{-9} cm^2, respectively, so we can deduce the conductivity value of 0.15 S/cm. The conductivity of the $(NH_4)_6V_{10}O_{28}\cdot 6H_2O$ nanorods is higher than that of self-assembling $(NH_4)_{0.5}V_2O_5\cdot 6H_2O$ nanowires ($\sim10^{-3}$ S/cm) [8] or rf-sputtered V_2O_5 (10^{-4}–10^{-3} S/cm) [12]. Obviously, the compounds contain V^{5+} and V^{4+} due to the existence of NH_4^+. Therefore, it can be accepted that electrical conduction from $(NH_4)_6V_{10}O_{28}\cdot 6H_2O$ nanorods proceeds via hopping between V^{5+} and V^{4+} impurity centers.

Interestingly, the $(NH_4)_6V_{10}O_{28}\cdot 6H_2O$ nanorod sample exhibits slightly nonlinear, symmetric current/voltage (*I/V*) characteristics. In order to further study the electrical conduction mechanism, we have simulated the *I–V* curve. It is found that the obtained characteristic is symmetrical and behaves linearly for electrical field lower than 425 V/cm. This behavior may be explained by the Ohmic mechanism of conductivity in the low electrical field. A further increase in the applied voltage results in an exponential behavior in the current mechanism. This is typical for Schottky or Poole–Frenkel structures. Since the thickness size of the nanorod is more than 50 nm, the tunnel current can be ignored. The following are the formula of Schottky and Poole–Frenkel emission [13]:

$$I_{SE} \propto T^2 \exp\left(\sqrt{\frac{e^3 V/\varepsilon}{kT}}\right) \tag{2}$$

$$I_{PFE} \propto V \exp\left(\sqrt{\frac{e^3 V/\varepsilon}{kT}}\right). \tag{3}$$

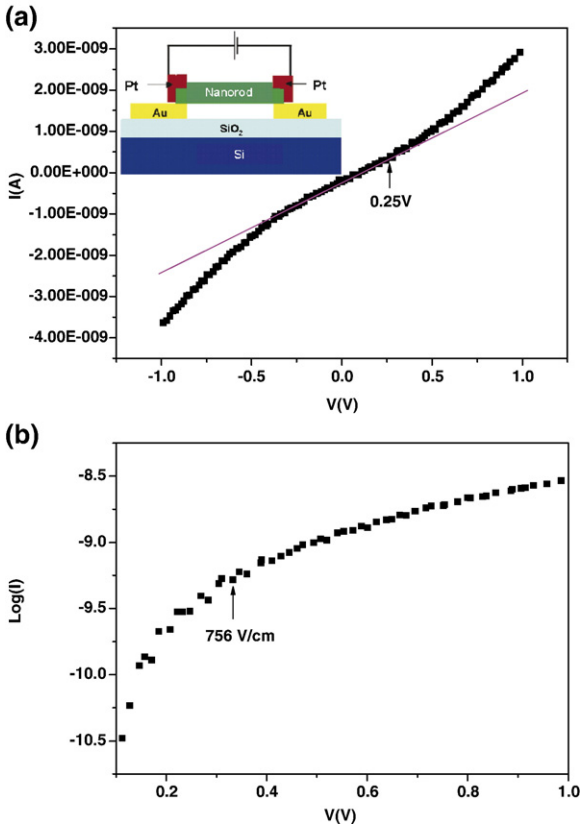

Fig. 4. (a) *I–V* curve of individual $(NH_4)_6V_{10}O_{28}\cdot 6H_2O$ nanorod (the inset is a schematic view of the individual nanorod electrode). (b) The positive part of the *I–V* characteristics of the transversal system, rebuild as a function of log(*I*).

Unlike the Schottky mechanism, defined by thermo-electron emission of the free charge carriers, the Poole–Frenkel transport is defined by emission from structural defects in energetic traps. The Poole–Frenkel mechanism is described by the following expression [14]:

$$I = qn_0 E \exp\left[-\frac{q}{kT}\left(\phi_B - \sqrt{\frac{qE}{\pi\varepsilon}}\right)\right] \quad (4)$$

where n_0 is the carrier density, q is the mobility of carriers, and ϕ_B is the depth of the traps in the $(NH_4)_6V_{10}O_{28}\cdot 6H_2O$ nanorods. The second component in the square brackets is equivalent to the Schottky barrier lowering due to the presence of an electric field. Fig. 4b presents the positive part of the I–V characteristics of the transversal system, rebuild as a function of log(I). The aim of this plot is to analyze the conduction mechanism in high fields (enlarged voltages). It is seen that the conductance behavior within fields that are lower than 756 V/cm, may be described as a Schottky behavior and right after this value as a Poole–Frenkel behavior. The $(NH_4)_6V_{10}O_{28}\cdot 6H_2O$ nanorods are found to have some bulk and surface defects, as shown by circles in Fig. 3e. Therefore, Poole–Frenkel emission in this case is the preferable mechanism that agrees with the results described by others [13].

4. Conclusions

In summary, $(NH_4)_6V_{10}O_{28}\cdot 6H_2O$ nanorods with the texture-like morphology were successfully synthesized. This is an efficient and mild solution method with clear advantages over the traditional high-temperature approach for the large-scale production of 1-D multicomponent nanomaterials. The individual $(NH_4)_6V_{10}O_{28}\cdot 6H_2O$ single crystalline nanorod exhibits nonlinear current/voltage (I/V) characteristics, with a conductivity of 0.15 S/cm at room temperature. The dominant conduction mechanism is based on small polaron hopping and the I–V curve consists of a linear, Ohmic regime at lower electrical field and a nonlinear one at higher electrical field. The increase of electronic conductivity of nanorods could be related to the reduction of oxidation state of vanadium from V^{5+} to V^{4+} corresponding to the chemical redshift of Raman peak at 913 cm^{-1}. The novel nanomaterials will exhibit potential applications in areas such as nanoelectrodes and other electrical devices.

Acknowledgements

This work was partly supported by the National Nature Science Foundation of China (50702039), Program for Changjiang Scholars and Innovative Research Team in University (PCSIRT, No. IRT0547), Ministry of Education, China, the Natural Science Foundation of Hubei Province (2006ABA310), and the Wuhan Youth Chenguang Project (20065004116-17). The author is pleased to thank the strong support of Prof W Chen, Prof ED Gu, Mr T Hu and Mr CS Lao.

References

[1] Z.W. Pan, Z.R. Dai, Z.L. Wang, Science 291 (2001) 1947.
[2] C.T. Kresge, M.E. Leonowicz, W.J. Roth, J.C. Vartuli, J.S. Beck, Nature 359 (1992) 710.
[3] S. Iijima, Nature 354 (1991) 56.
[4] S. Pavasupree, Y. Suzuki, A. Kitiyanan, S. Pivsa-Art, S. Yoshikawa, J. Solid State Chem. 178 (2005) 2152.
[5] K. Takahashi, Y. Wang, K. Lee, G. Cao, Appl. Phys., A 82 (2006) 27.
[6] K. Takahashi, S.J. Limmer, Y. Wang, G.Z. Cao, Japan. J. Appl. Phys. 44 (2005) 662.
[7] L.Q. Mai, B. Hu, T. Hu, W. Chen, E.D. Gu, J. Phys. Chem., B 110 (2006) 19083.
[8] X.C. Wu, Y.R. Tao, L. Dong, J.M. Hong, J. Mater. Chem. 14 (2004) 901.
[9] C.S. Lao, J. Liu, P.X. Gao, L.Y. Zhang, D. Davidovic, R. Tummala, Z.L. Wang, Nano Lett. 6 (2006) 263.
[10] W. Han, S.S. Fan, Q. Li, Phys. Lett. 265 (1997) 374.
[11] H.X. Li, L.F. Jiao, H.T. Yuan, M. Zhao, Y.M. Wang, Mater. Lett. 61 (2007) 101.
[12] F.P. Koffyberg, F.A. Benko, Philos. Mag., B 38 (1978) 357.
[13] P.P. Boriskov, A.A. Velichko, A.L. Pergament, G.B. Stefanovich, D.G. Stefanovich, Tech. Phys. Lett. 28 (2002) 406.
[14] G. Golan, A. Axelevitch, B. Sigalov, B. Gorenstein, J. Optoelectron. Adv. Mater. 6 (2004) 189.